atmosphere

MDPI

Article

Grain-Size End-Members of Anguli-Nuur Lake Core Sediments: Evidence for Moisture Variability in Northern China since the Last Deglaciation

Junfeng Li [1,2], Xingqi Liu [2,*], Xin Mao [2,3] and Huiqing Yang [1]

[1] College of Resource and Environment Sciences, Shijiazhuang University, Shijiazhuang 050035, China
[2] College of Resource Environment and Tourism, Capital Normal University, Beijing 100048, China
[3] Institute of Hydrogeology and Environmental Geology, Chinese Academy of Geological Sciences, Shijiazhuang 050061, China
* Correspondence: xqliu@cnu.edu.cn

Abstract: The common methods used for grain-size analysis have their own deficiencies and limitations in terms of explaining the genesis of grain-size components. In this study, the end-member modeling analysis method is applied to multi-mode grain-size distributions of core sediment from Anguli-nuur lake to help to understand the sediment provenance, transport processes and sedimentary environment. Four optimal end-members are unmixed, and three transport-deposition processes are revealed, including the runoff, wave and aeolian processes. The humidity index synthesized by the runoff and aeolian end-members in the core sediment is used to reconstruct the humidity variability in the East Asian monsoonal domain since the last deglaciation. Our record shows that the patterns of humidity variability are coincidentally linked with the monsoonal precipitation index from the same core and stalagmite record in southern China. The Holocene optimum is identified in early and middle Holocene. In addition, a series of millennial- and multi-centennial-scale dry events documented in our record are well correlated with the ice-rafted debris events in the North Atlantic. The results reveal that the grain-size record from Anguli-nuur lake is sensitive in response to moisture variability in northern China.

Keywords: grain-size distribution; last deglaciation; northern China; Anguli-nuur lake; Asian monsoon

check for updates

Citation: Li, J.; Liu, X.; Mao, X.; Yang, H. Grain-Size End-Members of Anguli-Nuur Lake Core Sediments: Evidence for Moisture Variability in Northern China since the Last Deglaciation. *Atmosphere* **2022**, *13*, 1826. https://doi.org/10.3390/atmos13111826

Academic Editors: Sridhara Nayak and Netrananda Sahu

Received: 29 September 2022
Accepted: 31 October 2022
Published: 2 November 2022

Publisher's Note: MDPI stays neutral with regard to jurisdictional claims in published maps and institutional affiliations.

Copyright: © 2022 by the authors. Licensee MDPI, Basel, Switzerland. This article is an open access article distributed under the terms and conditions of the Creative Commons Attribution (CC BY) license (https://creativecommons.org/licenses/by/4.0/).

1. Introduction

The grain-size distribution of lake sediments, which serves as a traditional proxy in paleoclimatic research, provides rich information about regional precipitation, lake-level fluctuations, dust-storm history and glacial advance-retreat processes [1–4]. The grain-size data of lake surficial sediment, such as mean size and standard deviation, could help people estimate sediment provenance, transport processes and sedimentary environments [5]. The common means for grain-size analysis include the traditional statistics method, the standard deviation partition method and the modern process method. The traditional statistics method usually provides descriptive statistics, such as the mean, median, kurtosis and skewness of grain-size distributions, which are probably biased for multi-mode and asymmetrical grain-size distributions [6,7]. The standard deviation partition method regards the size classes whose fractions have the highest variability as the environmentally sensitive components. These components are interpreted as indicators of regional humidity or drought and are associated with climate changes [8,9]. The modern process method establishes the relationship between the grain-size components of lake surface sediments and the specific sedimentary environment. Then, the identified components are applied to core sediments to reveal rich paleohydrological information for lakes [10,11].

In recent years, end-member (EM) modeling analysis for grain-size distributions has frequently been used in paleoclimatic and paleoenvironmental reconstruction [3,6,12,13].

This method can extract the independent transport-deposition EMs, with each EM representing a specific sedimentary process [7,14–16]. In Lake Zabinskie, Poland, decomposition of grain-size distributions with the EM method allows for the recognition of relative changes in the deposition of allochthonous (mineral) and autochthonous (carbonates, (hydr) oxides) components [17]. In this study, we present a well-dated grain-size record using end-member modeling analysis (EMMA) from Anguli-nuur lake in northern China to reconstruct the humidity variability in the Asian monsoonal domain since the last deglaciation. Based on the comparison with the precipitation proxy index in the same core, as well as the stalagmite records in southern China, and the ice-rafted debris events (i.e., Bond events) in the North Atlantic, we evaluate the grain-size record of Anguli-nuur lake in response to the moisture variability in northern China since the last deglaciation.

2. Materials and Methods

2.1. Study Area

Anguli-nuur lake (41°18′ N~41°24′ N, 114°20′ E~114°27′ E, 1315 m a.s.l.) is an inland saline lake located in the northern limit of the Asian summer monsoon (Figure 1a). The lake region is dominated by the Asian monsoon system, which is characterized by a warm-wet summer monsoon with precipitation from the Pacific Ocean in the southeast and a cold-dry winter monsoon from Siberia and Mongolia in the northwest [18]. Thus, this area is highly sensitive to climatic and environmental changes. The lake lies in a semi-arid region, which is approximately 120 km from the southern part of the Otindag Sandy Land of the Inner Mongolian Plateau (Figure 1b). The Heishui River from the east and Santai River from the south are the two main rivers that feed the lake (Figure 1c). The closed lake had a water surface area of 47.6 km^2, with a length of 11.6 km, a width of 4.1 km and an average depth of 2.5 m recorded in 1986 [19]. Because of the two artificial reservoirs that were built, the catchment area of Anguli-nuur lake shrank from 3495.0 km^2 to 722.4 km^2 in 1959. The lake has been completely desiccated since 2004, and the present basin surface is covered by white-colored saline efflorescence in winter. The annual mean temperature from 1981 to 2010 was 3.6 °C, and the mean monthly temperatures in January and July were −14.6 °C and 19.2 °C, respectively (Figure 1d). The annual mean precipitation is 383 mm, with 64% concentrated during June–August, which is one-fifth to one-quarter times the amount of the annual potential evaporation. From March to May, the monthly mean wind velocity usually exceeds 4 m/s, which transports dust into the lake [20].

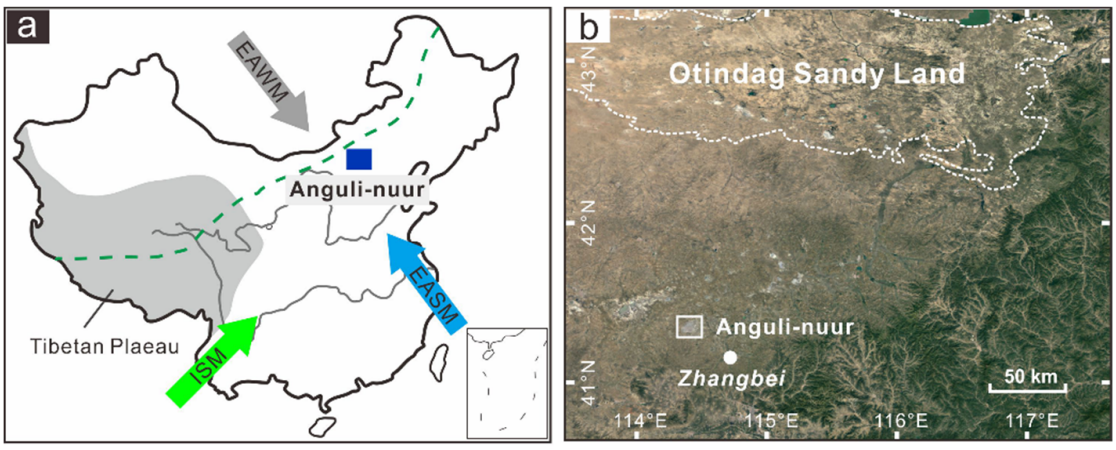

Figure 1. *Cont.*

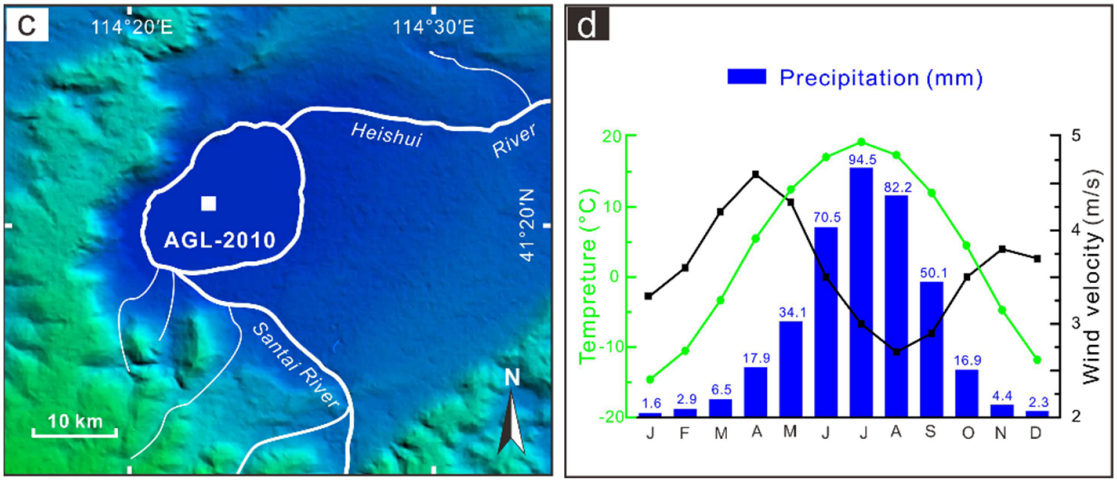

Figure 1. (**a**) Map of the study region in China. EASM is the East Asian summer monsoon, EAWM is the East Asian winter monsoon, and ISM is the India summer monsoon. The modern Asian summer monsoon limit is shown by the dashed green line. (**b**) Map of the Anguli-nuur lake region and the Otindag Sandy Land. (**c**) Map of the location of core AGL-2010. (**d**) Monthly mean precipitation, temperature, and wind velocity for the Zhangbei County meteorological station from 1981 to 2010 (http://data.cma.cn/ (accessed on 10 November 2021).

2.2. Core AGL-2010

In the autumn of 2010, a 38 m long sediment core, designated AGL-2010, was extracted from the center part of Anguli-nuur lake, using a modified XY-1B corer made in China (Figure 1c). The top part (0–60 cm) of core AGL-2010 was cut into 1 cm subsamples with the remaining part cut into 2 cm subsamples for laboratory analyses. In this paper, the upper 21.5 m, with reliable dates, was used for grain-size analysis. The base and upper parts of the sediments were composed of a grayish-yellow clayey silt and a grayish-green clay. The middle parts of the sediments consisted of a grayish and black clay. The core sediments contained abundant saline minerals, such as the stable mirabilite layers at 19.5–18.1 m, gypsum and bloedite crystals at 18.1–15.0 m and fine gaylussite crystals at 10.0–7.0 m (Figure 2) [21].

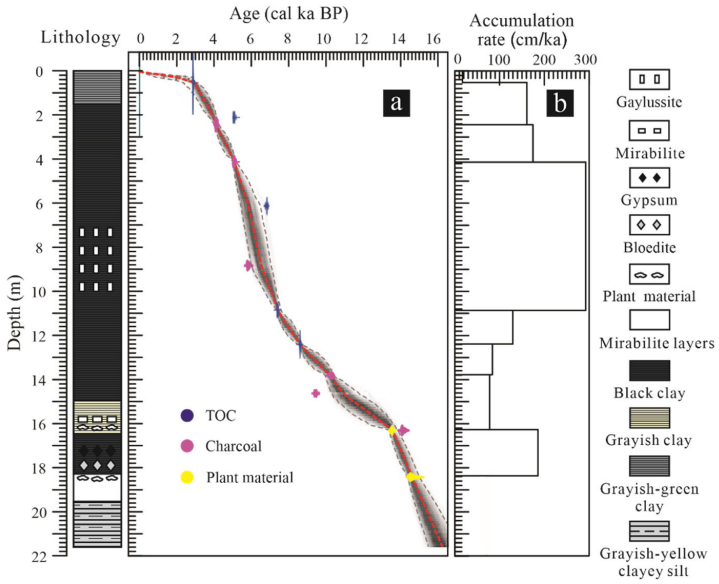

Figure 2. Lithology and geochronology of core AGL-2010 [21]. (**a**) Bayesian age-depth model [20]. (**b**) Sedimentation-rate histogram. Sedimentation rates are calculated between AMS ^{14}C ages that fall on the red dashed line.

2.3. Age-Depth Model

The age sequence is established by thirteen AMS ^{14}C dates, including two plant material dates, six charcoal dates and five sedimentary total organic carbon (TOC) dates (Table 1). The age of each subsample is established using the Bacon 2.2 program in R software [22] (Figure 2a). The $\delta^{13}C$ of the two plant materials are −10.2‰ and −10.7‰, respectively (Table 1), and the TOC/TN ratios from Anguli-nuur lake sediments typically exceed 10 [21], which indicates that the plant materials originate from terrestrial plants [23,24]. Charcoal is a product of vegetation fires and is usually not affected by carbon reservoir effects. Three TOC dates fall on the smooth age-depth line established using the plant material and charcoal dates, suggesting that these layers are less affected by the carbon reservoir effects. However, two older TOC dates at depths of 2.1 m and 6.1 m are rejected by the smooth age–depth line, suggesting that these two layers may be influenced by the old carbon effect. Thus, the age sequence of core AGL-2010 is relatively reliable, with an age of approximately 16.0 cal ka BP at the bottom. The sediment accumulation rates in the core are in the range of 17.8 to 293.2 cm/ka, with an average of 134.4 cm/ka (Figure 2b). This rate has become markedly slower during the past 3.0 cal ka BP, which is similar to the previous conclusion reported for Anguli-nuur lake [18]. It was also found that the higher percentages of silt (68.7%) in the upper 100 cm are in agreement with the lower sedimentation rate (Figure 3).

Table 1. AMS ^{14}C ages and calendar ages obtained for core AGL-2010.

Lab ID	Depth (cm)	Dated Material	^{14}C Age (a BP)	$\delta^{13}C$ (‰)	Calibrated Age (cal. a BP) (±2σ)
NZA 37124	49	TOC	2640 ± 20	−24.0	2744–2776
NZA 37144	211	TOC	4363 ± 25	−24.7	4858–4975
NZA 57912	241	Charcoal	3651 ± 21	−25.4	3897–3998
NZA 57913	411	Charcoal	4376 ± 20	−25.5	4866–4975
NZA 36953	611	TOC	5835 ± 25	−25.4	6601–6731
NZA 59224	880	Charcoal	4918 ± 52	−25.3	5582–5748
NZA 36954	1085	TOC	6296 ± 25	−25.6	7170–7266
NZA 50810	1238	TOC	7593 ± 31	−23.6	8357–8429
NZA 59157	1377	Charcoal	8891 ± 33	−25.4	9905–10,171
NZA 59770	1458	Charcoal	8250 ± 31	−24.8	9121–9322
NZA 57914	1627	Charcoal	11,965 ± 44	−19.0	13,712–13,999
NZA 58787	1627	Plant material	11,393 ± 43	−10.2	13,125–13,321
NZA 58788	1837	Plant material	12,314 ± 48	−10.7	14,074–14,624

2.4. Grain-Size Analysis

For grain-size analyses, 428 samples were pretreated with 10% H_2O_2 to remove organic matter and with 10% HCl to remove carbonates; the subsamples were then dispersed with 10 mL of 0.05 M $(NaPO_3)_6$ on an ultrasonic vibrator for 10 min. Grain-size distributions between 0.01 and 3000 µm were measured using a Malvern Mastersizer 3000 laser grain-size analyzer at Capital Normal University, Beijing, China.

2.5. End-Member Modeling Analysis

The original multi-mode grain-size data of core AGL-2010 were transferred into unmixed EMs using the EMMA method [15]. This method can extract genetically meaningful EM distributions and their scores from the whole core sediment. Then, each EM can be interpreted in terms of sediment provenance, transport processes, sedimentary environment and potential information about environmental and climatic changes [15].

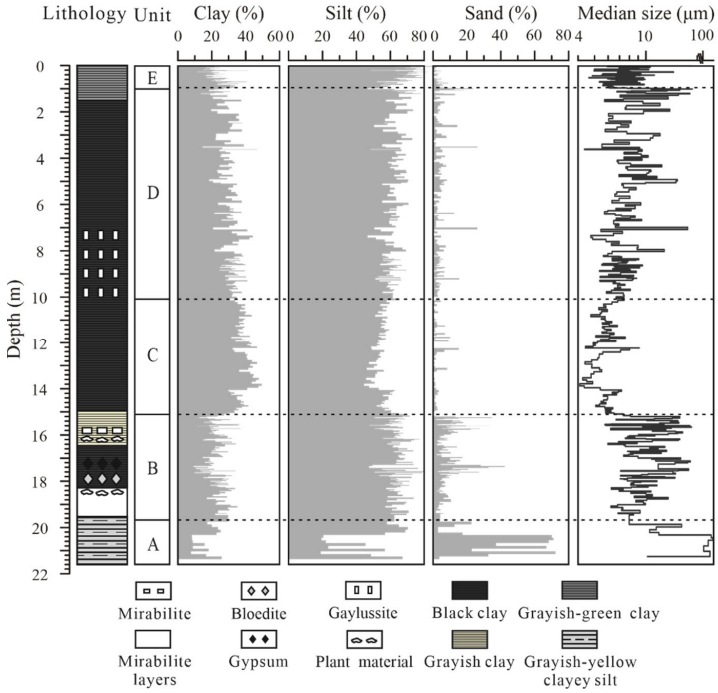

Figure 3. Variations in grain-size compositions and median size of core AGL-2010.

3. Results

Core AGL-2010 is mainly composed of clay and silt, with average percentages of 28.4% and 61.7%, respectively (Figure 3). Based on the feature of grain-size compositions and distribution in each interval, we divided the core sediment into five units (Figures 3 and 4).

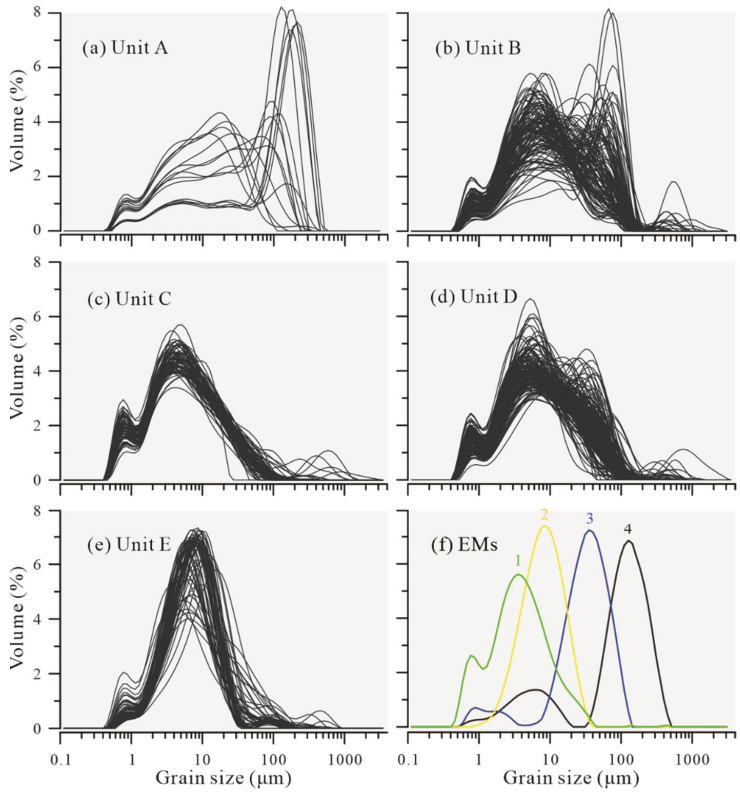

Figure 4. Frequency distribution curves of different units (**a**–**e**) and four EM curves (**f**) in core AGL-2010.

Unit A (21.5–19.75 m): the sand fraction accounts for an average of 35.8% (Figure 3), and the grain-size distribution shows a major mode between 100 and 400 μm (Figure 4a). Unit B (19.75–15.21 m): the silt fraction (63.7%) predominates this unit, and the median size fluctuates frequently and significantly (Figure 3). The multi-mode distribution characterizes this unit, with most subsamples possessing a mode grain size of approximately 4 μm, while a few subsamples have additional peaks between 30 μm and 60 μm (Figure 4b). Unit C (15.21–10.1 m): the clay (38.4%) reaches the maximum percentage, and the average median size is 5.9 μm (Figure 3). Meanwhile, this unit features a relatively uniform grain-size distribution with a mode size of approximately 4 μm (Figure 4c). Unit D (10.1–1.0 m): the percentage of silt fraction and median size values increase gradually (Figure 3). In addition, two mode grain-size distributions are exhibited in this unit, with most subsamples possessing a mode at 4 μm similar to that seen in Unit C and a few subsamples have a mode at 40 μm (Figure 4d). Unit E (1.0–0 m): this unit is dominated by the silt fraction (68.7%) (Figure 3), and the grain-size distribution is marked by a relatively uniform narrow peak at approximately 8 μm (Figure 4e). Obviously, the above five units show different grain-size distribution characteristics, which indicates that they experienced different sedimentary modes in different climatic conditions. A detailed discussion is presented in Section 4.2. Almost all of the grain-size distributions for core AGL-2010 were revealed to have a super-fine mode size of 0.7 μm (Figure 4), which may represent the background level of atmospheric aerosols in the arid region of northwestern China [25].

The different transport-deposition processes are unmixed by the EMMA method from the multi-mode grain-size distributions in core AGL-2010 [15]. The coefficient of determination (R^2) and mean angular deviation (θ) are calculated to identify the minimal numbers of EMs. Relatively higher R^2 and lower θ values suggest a better statistical fit [15]. When an EM number = 4, both R^2 (96.3%) and θ (7.3°) are turning slightly, implying that the 4-number model possibly satisfies the minimum required EM number in core AGL-2010 (Figure 5).

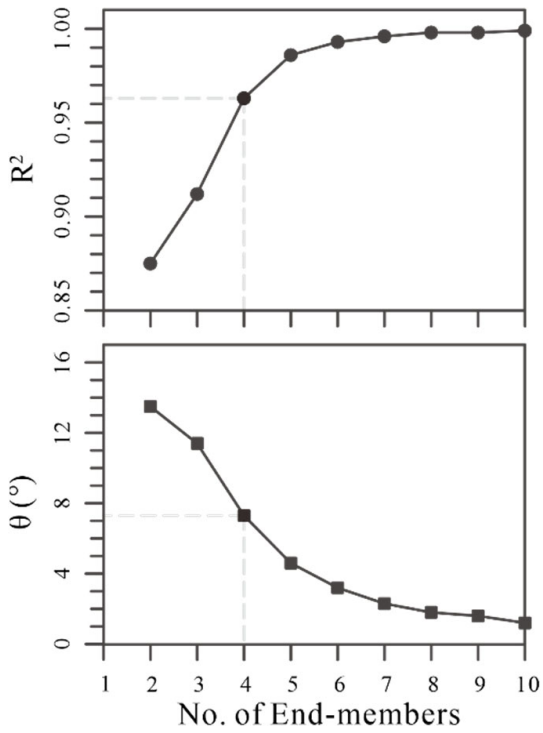

Figure 5. Coefficients of determination (R^2) and mean angular deviation (θ) as a function of the number of end-members for core AGL-2010.

4. Discussion

4.1. Implication of End-members in Anguli-Nuur Lake

In semi-arid and arid regions, seasonal runoffs with low discharge usually transport finer suspended particles, such as clay, to the central part of a lake, especially in a shallow and flat basin [12,26,27]. The grain-size distribution of EM1, which has a major mode at 3.6 μm, explains 41.7% of the total EM variance (Table 2; Figure 4f). This mode size is similar to that of the suspended component C2, in Hulun Lake [26] and Dali Lake [28]. These three lakes are all inland lakes, with a shallow flat basin and are all located in the northern limit of the Asian summer monsoon. Therefore, it suggests that EM1 probably represents the suspended component from fluvial and alluvial processes, which reaches a longer distance and accumulates under high lake levels and calm water conditions [3,6].

Table 2. Characteristics of the four EMs extracted from core AGL-2010. For the curves of each EM, see Figure 4f.

EMs	Mode Size (μm)	Variance (%)	Component Interpretation
EM1	3.6	41.7	Runoff suspension component
EM2	8.7	31.7	Storm-driven waves component
EM3	35.3	22.7	Aeolian suspension component
EM4	127.0	3.9	Nearshore aeolian saltation sand

The EM2 has a mode at 8.7 μm, which explains 31.7% of the total variance (Table 2; Figure 4f). EMs 2 and 1 show an obviously negative correlation ($r = -0.503$, $p = 0.01$, $n = 428$), suggesting EM2 and EM1 represent different transport-deposition dynamics. When EM2 predominates the variance, EM1 is weak and the lake level is low. Anguli-nuur Lake has a shallow flat basin. The size of a lake would decrease rapidly when the depth of a lake becomes shallower under drier climate conditions. In this condition, the offshore distance of the core site was shorter than before, and the coarser particles suspended by storm-driven wave processes would be transported from the shoreline to the center of lake more easily. Thus, we infer that EM2 probably represents the suspended component from shoreline materials that have been transported to the depocenter by storm-driven wave processes, especially when the offshore distance to the core site was short.

In the Anguli-nuur lake region, runoff is thought to be insufficient to transport coarse particles to the central part of the lake [29]. In contrast, the northwest wind prevails during winter and spring in the lake region. The highest speed is 28 m/s, and the average wind velocity exceeds 10.8 m/s for 50–70 days/year [20]; this wind velocity is high enough to transport aeolian dust into the lake [30]. The EM3 has a major mode at 35.3 μm and explains 22.7% of the total variance (Table 2; Figure 4f). The typical loess in China, e.g., Malan loess in Xi'an and Yulin, have similar characteristics to grain-size distribution [31]. The grain-size distributions of EM3 resemble those of the dominant suspended components of typical loess deposits [31–33], suggesting that EM3 is probably from the Sandy Land in the northwest and is transported by the aeolian suspension process.

EM4, the coarsest, has a major mode size of 127.0 μm and explains only 3.9% of the total EM variance (Table 2; Figure 4f); however, it is extremely centralized at the bottom of core AGL-2010 (Figure 6). EM4 might represent the dune component blown onto lake ice from nearshore areas by aeolian saltation processes in winter and spring [6]; this material then accumulates on the lake bottom when the ice melts.

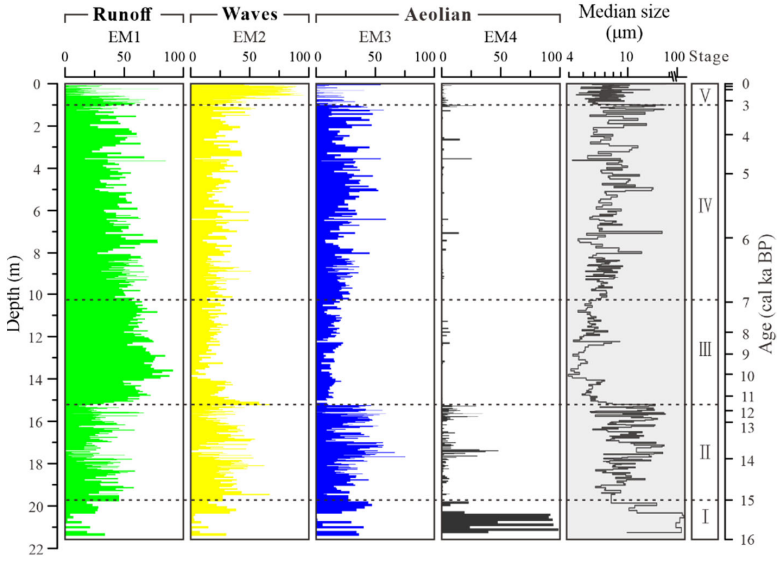

Figure 6. EM scores and median size of core AGL-2010.

4.2. Reconstruction of Dry-Wet Changes since the Last Deglaciation

Based on the AMS ^{14}C dating and the grain-size analysis of the core sediment of Anguli-nuur lake, the dry-wet changes in northern China since the last deglaciation can be classified into the following five stages (Figure 6).

Stage I (21.5–19.75 m, 16.0–15.0 cal ka BP): The score of EM1 is low, which shows the runoff was weak. The score of EM4 is the highest and the median size reaches the highest values with an average of 62 μm in the whole sequence, which clearly indicates that the aeolian sand dominated this stage (Figure 6). Based on these data, it can be inferred that a weak summer monsoon and extremely dry conditions with an active aeolian sand activity occurred at this stage.

Stage II (19.75–15.21 m, 15.0–11.5 cal ka BP): EM1 and EM3 alternately dominate this stage, and the median size fluctuates frequently and significantly, which indicates that the climate alternated between dry and wet, with frequent and abrupt fluctuations (Figure 6).

Stage III (15.21–10.1 m, 11.5–6.9 cal ka BP): The finest EM1 explains 63.3% of the variance, and the average median size is 5.9 μm with the smallest fluctuations (Figure 6). Therefore, wet conditions and high lake levels probably occurred in the early and middle Holocene.

Stage IV (10.1–1.0 m, 6.9–3.1 cal ka BP): EM1 gradually decreases, while EM3 and median size values gradually increase with greater fluctuations (Figure 6). According to these, the climate conditions were gradually turning to drought.

Stage V (1.0–0 m, 3.1–0 cal ka BP): EM1 further decreases and EM2 rapidly increases, explaining 61.7% of the variance (Figure 6). Therefore, the climate conditions were probably drier in the late Holocene. In addition, this stage exhibits an extremely low accumulation rate, with an average of 17 cm/ka (Figure 2b). Thus, we infer that the particles were mainly from the shoreline and were eroded by storm-driven waves. This process possibly occurred when the lake depth became shallower under drier climate conditions, with the size of the lake decreasing rapidly. In this condition, the offshore distance of the core site was shorter than before, and the coarser particles suspended by storm-driven wave processes could have been transported from the shoreline to the center of the lake more easily.

4.3. Linking End-Members to Humidity Variability

The transport capacity of runoff is directly related to the mean annual precipitation [10,12], that is, more monsoonal precipitation over a lake catchment leads to more fluvial suspended particles being deposited in the depocenter of a lake. The aeolian activities are usually related to droughts, that is, more aeolian components in core sediments indicate a drier lake

region [12,34]. Thus, we use [EM1− (EM3 + EM4)] as the humidity index (HI) of Anguli-nuur lake, i.e., a high HI score reflects the humidity over the lake region.

The humidity variability since the last deglaciation is evaluated by the HI score from core AGL-2010 (Figure 7a). Our reconstruction shows that the humidity variability over the lake region experienced three periods since the last deglaciation, including: (1) alternating dry and wet climate conditions were recorded in the last deglaciation, (2) the humidity variability increased abruptly at the beginning of the Holocene, and the Holocene optimum occurred in the early and middle Holocene, and (3) the climate gradually became drier in the middle and late Holocene. Based on the TOC content of the same sediment core (Figure 7b), the history of monsoonal precipitation since the last deglaciation was reconstructed [21]. Our HI records based on grain size show a positive correlation with the independent TOC records from the same core (Figure 7b, r = 0.402, p = 0.01, n = 428), and with the $\delta^{18}O$ values of stalagmites in monsoon-dominated southern China [35] (Figure 7c), suggesting that the humidity variability in Anguli-nuur lake is dominated by the Asian monsoon precipitation. The patterns of the humidity variability support the view that insolation is the primary factor that controls the regional hydrological variations in the Asian monsoonal domain [36].

In addition, millennial-scale dry events, such as the Oldest Dryas event and the Younger Dryas event, are recorded by the HI (Figure 7a). A series of multi-centennial-scale dry events are also clearly documented as having occurred at 14.0–13.6, 11.7–11.2, 10.5–10.2, 9.5–9.2, 8.6–8.2, 5.4–5.0, 4.5–4.2 and 3.6–3.1 cal ka BP; moreover, the events at 14.0–13.6 and 8.6–8.2 cal ka BP most likely correspond to the Older Dryas and the 8.2 ka events, respectively [37,38]. Not only do most of these events correspond well with the speleothem records in the Asian monsoonal domain [35,36], some are also more evident in our record than in speleothem records, such as the Older Dryas and 8.2 ka events [35] (Figure 7c). This evidence implies that the grain-size variations in the sediment of Anguli-nuur lake might be more sensitive to changes in monsoonal precipitation because of the large surface area and relatively shallow depth [26]. This series of dry events is well correlated with the Bond events in the North Atlantic during the Holocene [39] (Figure 7d). The consistencies in timing and phasing not only corroborate the validity of our age control but also strongly suggest that the variation in moisture in northern China on the millennial to multi-centennial scale could be directly related to changes in the North Atlantic climate [40].

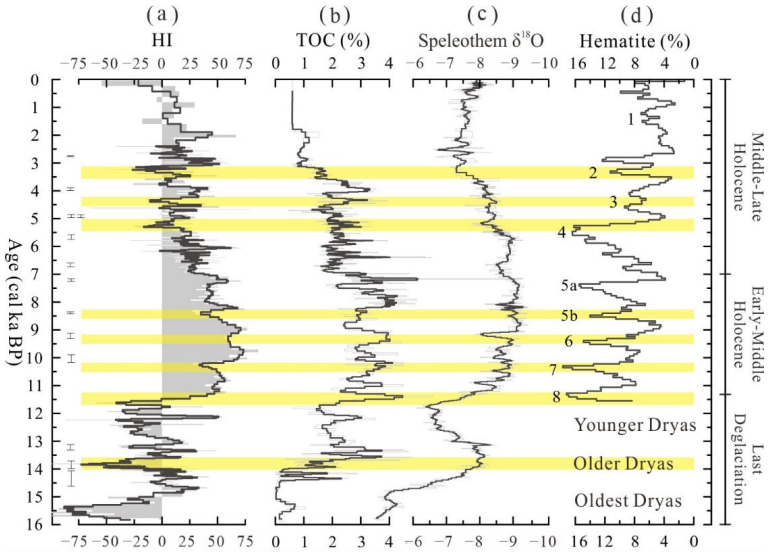

Figure 7. (**a**) Humidity index (HI) of core AGL-2010. The dark line represents the three-point running mean of the HI score. (**b**) TOC content of core AGL-2010 [21]. (**c**) Dongge Cave speleothem $\delta^{18}O$ records [35]. (**d**) Hematite-stained grain concentration from the North Atlantic [39]. Yellow bars mark dry events on a multi-centennial scale in Anguli-nuur lake.

In summary, the HI score exhibits a good correlation with the TOC content in the same core, as well as with the stalagmite record and the Bond events. Such a good agreement indicates that the grain-size record from Anguli-nuur lake is sensitive in response to moisture variability in northern China.

5. Conclusions

The grain-size EMMA method is used to study the provenance, transport processes and sedimentary environment of core sediment from Anguli-nuur lake. Our results show that four EMs are unmixed from the multi-mode grain-size distribution and that their scores are extracted from the whole core sediment. In terms of sedimentary dynamics, three transport processes are revealed, including the runoff, wave and aeolian processes.

The HI synthesized by runoff and aeolian EMs in core AGL-2010 is used to reconstruct the humidity variability since the last deglaciation. The Holocene optimum is identified in early and middle Holocene, which is in agreement with previous conclusions from the same core. Meanwhile, our records document a series of millennial- and multi-centennial-scale dry events, which are well correlated with the Bond events in the North Atlantic. These good correlations indicate that the grain-size record from Anguli-nuur lake is sensitive in response to climate change in northern China.

Anguli-nuur lake lies about 120 km from south of the Otindag Sandy Land, Inner Mongolia, where the northwest winds prevail in spring. In the AGL-2010 core, sand and silt contents exceed 70%, and two robust aeolian EMs have been extracted in this study. This provides good foundations to further explore the relationship between aeolian sand activity and humidity changes in northern China since the last deglaciation.

Author Contributions: J.L.: data curation, funding acquisition, investigation, writing-original draft, writing-review & editing; X.L.: funding acquisition, project administration, resources, supervision, writing-review & editing; X.M.: formal analysis, software; H.Y.: validation. All authors have read and agreed to the published version of the manuscript.

Funding: This work was supported by the National Key R&D program of China (Grant No. 2018YFA0606404), the National Natural Science Foundation of China (Grant No. 41372176) and the Doctoral Startup Foundation of Shijiazhuang University (Grant No. 20BS028).

Institutional Review Board Statement: Not applicable.

Informed Consent Statement: Not applicable.

Data Availability Statement: Not applicable.

Acknowledgments: We thank Zhitong Yu for their help with fieldwork. We thank Yongbo Wang for providing the end-memeber modeling algorithm.

Conflicts of Interest: The authors declare no conflict of interest.

References

1. Peng, Y.; Xiao, J.; Nakamura, T.; Liu, B.; Inouchi, Y. Holocene East Asian monsoonal precipitation pattern revealed by grain-size distribution of core sediments of Daihai Lake in inner Mongolia of north-central China. *Earth Planet. Sci. Lett.* **2005**, *233*, 467–479. [CrossRef]
2. Qiang, M.; Chen, F.; Zhang, J.; Zu, R.; Jin, M.; Zhou, A.; Xiao, S. Grain size in sediments from Lake Sugan: A possible linkage to dust storm events at the northern margin of the Qinghai-Tibetan Plateau. *Environ. Geol.* **2007**, *51*, 1229–1238. [CrossRef]
3. Dietze, E.; Wünnemann, B.; Hartmann, K.; Diekmann, B.; Jin, H.; Stauch, G.; Yang, S.; Lehmkuhl, F. Early to mid-Holocene lake high-stand sediments at Lake Donggi Cona, northeastern Tibetan Plateau, China. *Quat. Res.* **2013**, *79*, 325–336. [CrossRef]
4. Liu, X.; Herzschuh, U.; Wang, Y.; Kuhn, G.; Yu, Z. Glacier fluctuations of Muztagh Ata and temperature changes during the late holocene in westernmost Tibetan Plateau, based on glaciolacustrine sediment records. *Geophys. Res. Lett.* **2014**, *41*, 6265–6273. [CrossRef]
5. Thomas, R.; Kemp, A.; Lewis, C. Distribution, composition and characteristics of the surficial sediments of Lake Ontario. *J. Sediment. Res.* **1972**, *42*, 66–84. [CrossRef]
6. Dietze, E.; Hartmann, K.; Diekmann, B.; Ijmker, J.; Lehmkuhl, F.; Opitz, S.; Wünnemann, B.; Borchers, A. An end-member algorithm for deciphering modern detrital processes from lake Sediments of Lake Donggi Cona, NE Tibetan Plateau, China. *Sediment. Geol.* **2012**, *243–244*, 169–180. [CrossRef]

7. Yu, S.Y.; Colman, S.M.; Li, L. BEMMA: A hierarchical bayesian end-member modeling analysis of sediment grain-size distributions. *Math. Geosci.* **2016**, *48*, 723–741. [CrossRef]
8. Boulay, S.; Colin, C.; Trentesaux, A.; Pluquet, F.; Bertaux, J.; Blamart, D.; Buehring, C.; Wang, P. Mineralogy and Sedimentology of Pleistocene Sediment in the South China Sea (ODP Site 1144). In Proceedings of the Ocean Drilling Program Scientific Results; Ocean Drilling Program: College Station, TX, USA, 2003; pp. 1–21. [CrossRef]
9. Liu, J.; Wang, Y.; Li, T.; Tian, F.; Yang, J. Comparison of grain-size distributions between nearshore sections and a deep-water sediment core from Dali Lake, North China, and inferred Holocene lake-level changes. *J. Paleolimnol.* **2016**, *56*, 123–135. [CrossRef]
10. Xiao, J.; Fan, J.; Zhou, L.; Zhai, D.; Wen, R.; Qin, X. A model for linking grain-size component to lake level status of a modern clastic lake. *J. Asian Earth Sci.* **2013**, *69*, 149–158. [CrossRef]
11. Xiao, J.; Fan, J.; Zhai, D.; Wen, R.; Qin, X. Testing the model for linking grain-size component to lake level status of modern clastic lakes. *Quat. Int.* **2015**, *355*, 34–43. [CrossRef]
12. Liu, X.; Dong, H.; Yang, X.; Herzschuh, U.; Zhang, E.; Stuut, J.; Wang, Y. Late Holocene forcing of the Asian winter and summer monsoon as evidenced by proxy records from the northern Qinghai-Tibetan Plateau. *Earth Planet. Sci. Lett.* **2009**, *280*, 276–284. [CrossRef]
13. Zhao, Y.; An, C.B.; Mao, L.; Zhao, J.; Tang, L.; Zhou, A.; Li, H.; Dong, W.; Duan, F.; Chen, F. Vegetation and climate history in arid western China during MIS2: New insights from pollen and grain-size data of the Balikun Lake, eastern Tien Shan. *Quat. Sci. Rev.* **2015**, *126*, 112–125. [CrossRef]
14. Weltje, G.J. End-member modeling of compositional data: Numerical-statistical algorithms for solving the explicit mixing problem. *Math. Geol.* **1997**, *29*, 503–549. [CrossRef]
15. Paterson, G.A.; Heslop, D. New methods for unmixing sediment grain size data. *Geochem. Geophys. Geosyst.* **2015**, *16*, 4494–4506. [CrossRef]
16. Zhang, X.; Zhou, A.; Wang, X.; Song, M.; Zhao, Y.; Xie, H.; Russell, J.M.; Chen, F. Unmixing grain-size distributions in lake sediments: A new method of endmember modeling using hierarchical clustering. *Quat. Res.* **2018**, *89*, 365–373. [CrossRef]
17. Zarczynski, M.; Szmanda, J.; Tylmann, W. Grain-size distribution and structural characteristics of varved sediments from Lake Zabinskie (Northeastern Poland). *Quaternary* **2019**, *2*, 8. [CrossRef]
18. Liu, H.; Yin, Y.; Zhu, J.; Zhao, F.; Wang, H. How did the forest respond to Holocene climate drying at the forest-steppe ecotone in northern China? *Quat. Int.* **2010**, *227*, 46–52. [CrossRef]
19. Wang, S.; Dou, H. *Lakes in China*; Chinese Science Press: Beijing, China, 1998; pp. 311–312. ISBN 7502741003.
20. Zhai, Q.; Guo, Z.; Li, Y.; Li, R. Annually laminated lake sediments and environmental changes in Bashang Plateau, North China. *Palaeogeogr. Palaeoclimatol. Palaeoecol.* **2006**, *241*, 95–102. [CrossRef]
21. Li, J.; Liu, X. Orbital- and suborbital-scale changes in the East Asian summer monsoon since the last deglaciation. *Holocene* **2018**, *28*, 1216–1224. [CrossRef]
22. Blaauw, M.; Christen, J.A. Flexible paleoclimate age-depth models using an autoregressive gamma process. *Bayesian Anal.* **2011**, *6*, 457–474. [CrossRef]
23. Krishnamurthy, R.V.; Bhattacharya, S.K.; Kusumgar, S. Palaeoclimatic changes deduced from $^{13}C/^{12}C$ and C/N ratios of Karewa lake sediments, India. *Nature* **1986**, *323*, 150–152. [CrossRef]
24. Meyers, P.A.; Ishiwatari, R. Organic matter accumulation records in lake sediments. In *Physics and Chemistry of Lakes*; Springer: Berlin, Germany, 1995; Volume 184, pp. 279–328. [CrossRef]
25. Xiao, S.; Chen, F.; Qiang, M.; Zhang, J.; Zhou, A.; Sun, D. Distribution pattern of grain size in surface sediments from Sugan Lake and its potential in recording aeolian dust in Arid China. *Acta Geogr. Sin.* **2007**, *62*, 1153–1164. [CrossRef]
26. Xiao, J.; Chang, Z.; Wen, R.; Zhai, D.; Itoh, S.; Lomtatidze, Z. Holocene weak monsoon intervals indicated by low lake levels at Hulun Lake in the monsoonal margin region of northeastern inner Mongolia, China. *Holocene* **2009**, *19*, 899–908. [CrossRef]
27. An, Z.; Colman, S.M.; Zhou, W.; Li, X.; Brown, E.T.; Jull, A.J.T.; Cai, Y.; Huang, Y.; Lu, X.; Chang, H.; et al. Interplay between the westerlies and Asian monsoon recorded in Lake Qinghai sediments since 32 ka. *Sci. Rep.* **2012**, *2*, 619. [CrossRef] [PubMed]
28. Xiao, J.; Chang, Z.; Si, B.; Qin, X.; Itoh, S.; Lomtatidze, Z. Partitioning of the grain-size components of Dali Lake core sediments: Evidence for lake-level changes during the Holocene. *J. Paleolimnol.* **2009**, *42*, 249–260. [CrossRef]
29. Yin, Y.; Liu, H.; He, S.; Zhao, F.; Zhu, J.; Wang, H.; Liu, G.; Wu, X. Patterns of local and regional grain size distribution and their application to Holocene climate reconstruction in semi-arid inner Mongolia, China. *Palaeogeogr. Palaeoclimatol. Palaeoecol.* **2011**, *307*, 168–176. [CrossRef]
30. Wu, Z. *Aeolian Sand Geomorphology*; Chinese Science Press: Beijing, China, 1987; pp. 1–316.
31. Sun, D.; Lu, H.; David, R.; Sun, Y.; Wu, S. Bimode grain-size distribution of Chinese Loess and its paleoclimate implication. *Acta Sedimentol. Sinica.* **2000**, *3*, 327–335. [CrossRef]
32. Tsoar, H.; Pye, K. Dust transport and the question of desert loess formation. *Sedimentology* **1987**, *34*, 139–153. [CrossRef]
33. Qin, X.; Cai, B.; Liu, T. Loess record of the aerodynamic environment in the East Asia monsoon area since 60,000 years before present. *J. Geophy. Res.* **2005**, *110*, B01204. [CrossRef]
34. Xu, B.; Wang, L.; Gu, Z.; Hao, Q.; Wang, H.; Chu, G.; Jiang, D.; Liu, Q.; Qin, X. Decoupling of climatic drying and Asian dust export during the Holocene. *J. Geophy. Res.* **2018**, *123*, 915–928. [CrossRef]

35. Dykoski, C.; Edwards, R.; Cheng, H.; Yuan, D.; Cai, Y.; Zhang, M.; Lin, Y.; Qing, J.; An, Z.; Revenaugh, J. A high-resolution, absolute-dated Holocene and deglacial Asian monsoon record from Dongge Cave, China. *Earth Planet. Sci. Lett.* **2005**, *233*, 71–86. [CrossRef]
36. Wang, Y.; Cheng, H.; Edwards, R.L.; He, Y.; Kong, X.; An, Z.; Wu, J.; Kelly, M.J.; Dykoski, C.A.; Li, X. The Holocene Asian monsoon: Links to solar changes and North Atlantic climate. *Science* **2005**, *308*, 854–857. [CrossRef] [PubMed]
37. Thomas, E.R.; Wolff, E.W.; Mulvaney, R.; Steffensen, J.P.; Johnsen, S.J.; Arrowsmith, C.; White, J.; Vaughn, B.; Popp, T. The 8.2 ka event from Greenland ice cores. *Quat. Sci. Rev.* **2007**, *26*, 70–81. [CrossRef]
38. Mangerud, J.; Briner, J.P.; Goslar, T.; Svendsen, J.I. The Bølling-age Blomvåg beds, western Norway: Implications for the Older Dryas glacial re-advance and the age of the deglaciation. *Boreas* **2016**, *46*, 162–184. [CrossRef]
39. Bond, G.; Kromer, B.; Beer, J.; Muscheler, R.; Evans, M.N.; Showers, W.; Hoffmann, S.; Lotti-Bond, R.; Hajdas, I.; Bonani, G. Persistent solar influence on North Atlantic climate during the Holocene. *Science* **2001**, *294*, 2130–2136. [CrossRef]
40. Porter, S.C.; Zhou, W. Synchronism of Holocene East Asian monsoon variations and North Atlantic drift-ice tracers. *Quat. Res.* **2006**, *65*, 443–449. [CrossRef]